

August 01, 2010

An experimental examination of mass perturbation strategies to mode normalization in a plate

Matthew Maddalo
Northeastern University

Recommended Citation

Maddalo, Matthew, "An experimental examination of mass perturbation strategies to mode normalization in a plate" (2010). *Civil Engineering Master's Theses*. Paper 18. <http://hdl.handle.net/2047/d20002087>

This work is available open access, hosted by Northeastern University.

**An Experimental Examination of Mass Perturbation Strategies to Mode
Normalization in a Plate**

A Thesis Presented

by

Matthew Maddalo

to

The Department of Civil and Environmental Engineering

in partial fulfillment of the requirements
for the degree of

Master of Science

in

Structural Engineering

Northeastern University
Boston, Massachusetts

August 2010

ABSTRACT

In modal identification, there are often practical applications where input forces cannot be determined, and output-only analysis must be implemented. A limitation of output-only identification is that the scaling which connects eigenvectors to the input-output response of the system is unknown. One particular strategy to obtain this normalization involves introducing a known perturbation to the system in question – typically a change in mass. Existing techniques operate under the assumption that the eigenvectors of the system are real, meaning that the system is undamped or classically damped. Although this often provides a reasonable approximation, it is never strictly true. In this thesis, an approach is outlined which calculates the required scaling factors without the assumption of classical damping. Specifically, the method solves for the scaling factors from an over-determined system of equations generated by evaluating the pole residue form of the Receptance matrix at the poles of the perturbed system. This new approach was verified through an experimental program on an aluminum plate, and the results compared favorably to those of other mode normalization techniques.

ACKNOWLEDGEMENTS

First and foremost, I would like to thank my advisor, Dr. Dionisio Bernal, whose guidance and accessibility throughout my experience at Northeastern has been invaluable. Anything I have accomplished at the graduate level has been due to his truly special ability to explain, to assist, and to challenge.

I must also thank Alyson Stuer, who was an important part of the preliminary study that served as the groundwork for this thesis. Her contributions are greatly appreciated.

The work presented in this thesis was made possible by the Intelligent Diagnostics IGERT program, funded by the National Science Foundation. I would like to express my sincere gratitude to the program director, Dr. Sara Wadia-Fascetti, and all the others who have supported my studies through the IGERT program.

NOMENCLATURE

C_d	Damping matrix
f	Frequency (Hertz)
$f(s)$	System input in Laplace domain
$f(t)$	System input in time domain
$G(s)$	Receptance, or transfer matrix
I	Identity matrix
i	Imaginary unit
K	Stiffness matrix
M	Mass matrix
m	Number of measurements
N	System Order
$q(s)$	System output in Laplace domain
$q(t)$	System output in time domain
s	Laplace variable
t	Time variable
x	State vector
α	Modal scaling factor for particular mode
$\hat{\alpha}$	Diagonal matrix containing all modal scaling factors
$\bar{\alpha}$	Column containing all modal scaling factors
β	Mass perturbation magnitude
ζ	Critical damping ratio
Θ	Matrix containing complex eigenvectors (length $2N$)
θ	Individual complex eigenvector (length $2N$)
Λ	Diagonal matrix containing all complex eigenvalues
λ	Individual complex eigenvalue
Φ	Matrix containing undamped mode shapes
ϕ	Column containing a single undamped mode shape

Ψ	Matrix containing complex mode shapes
ψ	Column containing a single complex mode shape
ω	Undamped frequency
ω_d	Damped frequency
$(\cdot)_0$	Relates to system parameters in original condition
$(\cdot)_1$	Relates to system parameters in mass perturbed condition
$(\cdot)^{-\dagger}$	Pseudoinverse
$(\cdot)^T$	Transpose
$vec(\cdot)$	Stacking operator
MAC	Modal Assurance Criterion

CONTENTS

ABSTRACT	i
ACKNOWLEDGEMENTS	ii
NOMENCLATURE.....	iii
CONTENTS	v
LIST OF FIGURES.....	vi
CHAPTER 1 – INTRODUCTION.....	1
1.1 Background and Motivation	1
1.2 Broader Impacts	2
CHAPTER 2 – MODAL THEORY FUNDAMENTALS.....	4
2.1 Introduction.....	4
2.2 The Classically Damped Case.....	4
2.3 The Arbitrarily Damped Case.....	8
CHAPTER 3 – MASS PERTURBATION THEORY	14
3.1 Introduction.....	14
3.2 Parloo Expression	14
3.3 Brincker and Andersen Expression.....	16
3.4 Bernal Projection Expression.....	18
3.5 Receptance Method	21
3.6 Summary of Methods	25
3.7 Normalization Example.....	26
CHAPTER 4 - EXPERIMENTAL CAMPAIGN.....	29
4.1 Introduction.....	29
4.2 Test Setup and Identification Procedure	29
4.3 Forced Vibration Test Results and Verification	31
4.4 Preliminary Studies.....	33
4.5 Operational Tests and Implementation of Methods.....	35
4.6 Results and Comparison of Methods.....	38
CHAPTER 5 – SUMMARY AND CONCLUSIONS	41
REFERENCES.....	43
APPENDIX.....	44

LIST OF FIGURES

<i>Figure 1: Photograph of plate with accelerometer configuration (red) and excitation location</i>	30
<i>Figure 2: Stabilization diagram for pole selection in LMS Test.Lab software</i>	31
<i>Figure 3: Shaker setup for forced vibration test</i>	32
<i>Figure 4: Frequency response function comparison - measured directly vs. generated from identification results (shaker to point 3)</i>	33
<i>Figure 5: Photograph of piezoelectric wafer actuator glued to plate surface (pictured with dime to show relative size)</i>	36
<i>Figure 6: Comparison of shaker modes to modes normalized with Receptance method</i>	40

LIST OF TABLES

<i>Table 1: Test mode set selected from forced vibration data</i>	32
<i>Table 2: Summary of Error Margins for Selected Frequencies</i>	34
<i>Table 3: Frequency shift results for various mass modifications (Abaqus model)</i>	35
<i>Table 4: Comparison of forced vibration and operational parameters</i>	37
<i>Table 5: Frequency shifts for various mass modifications (experimental data)</i>	37
<i>Table 6: Comparison of mode normalization methods (% error)</i>	39

CHAPTER 1 – INTRODUCTION

1.1 Background and Motivation

In modal testing, there are many structures and conditions that require the use of output-only identification. While a forced vibration test with a measured input may be ideal, it is not feasible in some practical applications. For example, if one wants to investigate the modal properties of an airplane wing or offshore structure while under service loading, obtaining a useful and accurate measurement of the inputs is difficult, if not impossible. Even in the case of a stationary civil structure where a shaker input is possible, it is not feasible to isolate the system from additional ambient excitation (e.g. wind loads). In situations such as these, modal parameters can be obtained by exposing the structure to its ambient service loading and performing identification with measured outputs only. This type of test is convenient in that the structure – a bridge, for example – can remain in service during the testing, which allows for significantly longer testing times and more accurate modal results. Also, since no instrumentation is required to excite the structure, the cost of equipment is reduced and the size of larger structures is less prohibitive of identification [1].

Although the use of output-only, or operational, testing can be advantageous for a variety of reasons, there is a major limitation associated with the lack of deterministic information on the input. While the frequencies, damping ratios, and mode shapes are available through output-only identification, the scaling which connects the mode shapes to the input-output response of the physical system is unknown. Properly scaled modes are required for a number of applications, including system response simulation and damage localization strategies based on flexibility changes [2]. This thesis explores methods which have previously been proposed to obtain the necessary modal scaling factors by introducing a mass perturbation and repeating the output-only identification [3-5]. A new Receptance-based technique is also explained, which uses a similar strategy of

mass perturbation, but does not rely on the assumption of a classically damped system, as prior methods have [6].

Experimental verification of operational mode shape normalization methods has typically focused on structures with low frequency modes, such as bridges or concrete slabs [7,8], although effectiveness has also been demonstrated using a beam-like structure [3]. In this thesis, the efficacy of various normalization techniques at higher frequencies is investigated experimentally through identification of an aluminum plate.

1.2 Broader Impacts

The work done for this thesis was made possible by a National Science Foundation grant directed at studying and developing Intelligent Diagnostics for Aging Infrastructure. As bridges, buildings, and other structures progress through their service lives, it is important to have some type of structural health monitoring. Whether the system involves visual inspection, complex equipment, or a combination of both, the behavior and condition of a structure must be assessed regularly. As mentioned in the previous section, output-only modal identification is a very attractive option for monitoring of civil structures. When considering infrastructure monitoring, it is clear that having a deterministic input for these systems, which tend to be quite large, may be cost and labor prohibitive. Additionally, suspending the service of a bridge or other structure to isolate the input loading has obvious drawbacks from the larger perspective of an efficient infrastructure system.

Therefore, it is important that output-only identification techniques continue to be developed with an eye toward structural health monitoring on a large scale. The ability to reliably obtain modal parameters of a civil structure while in service is a valuable tool from both safety assurance and maintenance prioritization points of view. Of course the advantages and convenience of output-only identification do not come without an information cost. The lack of knowledge regarding the

excitation of a structure puts a significant restraint on the information that can be obtained from one test. Developing methods to recover this information through multiple tests is a key step toward making the implementation of output-only testing a practical reality for damage assessment and maintenance prioritization. Adding intelligent vibration testing to existing standards of visual inspection can lead to both more reliable structural health assessment and more effective deployment of maintenance resources.

CHAPTER 2 – MODAL THEORY FUNDAMENTALS

2.1 Introduction

In this chapter, the fundamental relationships between system matrices and modal models are explained. The relevant theory is discussed for both the special case of classical damping (Section 2.2) and the more general case of arbitrary damping (Section 2.3).

2.2 The Classically Damped Case

For a system with N degrees of freedom, the dynamic equilibrium equation is as follows

$$M\ddot{q}(t) + C_d\dot{q}(t) + Kq(t) = f(t) \quad (1)$$

where M , C_d , and $K \in R^{N \times N}$ are the mass, damping, and stiffness matrices, respectively, and $f(t)$ are the applied loads. If a change of basis is performed such that $q = \Phi Y$, then one has

$$M\Phi\ddot{Y} + C_d\Phi\dot{Y} + K\Phi Y = f(t) \quad (2)$$

Premultiplying by Φ^T gives

$$\Phi^T M \Phi \ddot{Y} + \Phi^T C_d \Phi \dot{Y} + \Phi^T K \Phi Y = \Phi^T f(t) \quad (3)$$

There always exists a transformation, Φ , such that the first and third terms of this equation are diagonal. These are known as the undamped mode shapes, and their aforementioned property can be proven through examination of the undamped equilibrium equation for an unloaded condition, written as

$$M\ddot{q} + Kq = 0 \quad (4)$$

The solution for q takes the form

$$q = \phi e^{i\omega t} \quad (5)$$

and so substituting into Equation (4) gives

$$(-M\omega^2 + K)\phi e^{i\omega t} = 0 \quad (6)$$

Since the exponential term cannot equal zero, the solution becomes

$$K\phi = M\phi\omega^2 \quad (7)$$

where the solution vectors ϕ are the undamped mode shapes and the corresponding ω values are the undamped frequencies. Examining the j and k solutions to this equation,

$$K\phi_j = M\phi_j\omega_j^2 \quad (8)$$

$$K\phi_k = M\phi_k\omega_k^2 \quad (9)$$

one can premultiply the equation for the j solution by ϕ_k , and vice versa

$$\phi_k^T K \phi_j = \phi_k^T M \phi_j \omega_j^2 \quad (10)$$

$$\phi_j^T K \phi_k = \phi_j^T M \phi_k \omega_k^2 \quad (11)$$

Since the expressions in Equations (10) and (11) represent scalars, it is true that

$$\phi_k^T M \phi_j (\omega_k^2 - \omega_j^2) = 0 \quad (12)$$

Looking at different modes and accepting that there are no repeated frequencies, i.e., $\omega_j \neq \omega_k$, one concludes that

$$\phi_k^T M \phi_j = 0 \quad (13)$$

for $j \neq k$. The same proof can be executed to show that this holds true for the matrix K . Therefore, as stated previously, the undamped modes of the system diagonalize the mass and stiffness matrices, which can be represented as

$$\Phi^T M \Phi = \bar{d}_m \quad (14)$$

$$\Phi^T K \Phi = \bar{d}_k \quad (15)$$

and from Equation (7), it also clear that

$$\bar{d}_{k,j} = \bar{d}_{m,j} \omega_j^2 \quad (16)$$

When the damping is assumed to be classical, then the mode shapes diagonalize the damping matrix in a similar way, namely

$$\Phi^T C_d \Phi = \bar{d}_e \quad (17)$$

where

$$\bar{d}_{e,j} = \bar{d}_{m,j} (2\omega_j \zeta_j) \quad (18)$$

In this equation, ζ_j represents the percent of critical damping on mode j .

Combining the results of these equations, and examining the case of mass normalization where $\bar{d}_m = I$, Equation (3) can be uncoupled as

$$\ddot{Y}_j + 2\omega_j \zeta_j \dot{Y}_j + \omega_j^2 Y_j = \phi_j^T f(t) \quad (19)$$

for mode j . In modal identification, the parameters that one tries to obtain are those shown in Equation (19) – the mode shape (ϕ), the undamped frequency (ω), and the damping ratio (ζ).

There are many ways in which the modal parameters obtained from identification can be used. One key application is to use the results to calculate the Receptance. This quantity can be used to compute the output response of the system to various loadings. Taking a Laplace transform of Equation (19) gives

$$s^2 Y_j(s) + s \cdot 2\omega_j \zeta_j Y_j(s) + \omega_j^2 Y_j(s) = \phi_j^T f(s) \quad (20)$$

which can be solved for $Y_j(s)$ to yield

$$Y_j(s) = \frac{1}{(s^2 + s \cdot 2\omega_j \zeta_j + \omega_j^2)} \phi_j^T f(s) \quad (21)$$

Remembering from earlier that $q = \Phi Y$, one finds

$$q(s) = \sum_{j=1}^N \frac{\phi_j \phi_j^T}{(s^2 + s \cdot 2\omega_j \zeta_j + \omega_j^2)} f(s) \quad (22)$$

In this way, the obtained modal model can be used to calculate the response of a system to any load in the Laplace domain. The results can then be transformed to the real domain to produce a time history of the predicted output. The matrix represented in Equation (22) by the summation provides a linear map between the input, $f(s)$, and output, $q(s)$, of the system. It is commonly called the Receptance (or transfer matrix) and is often denoted by $G(s)$, such that

$$q(s) = G(s) f(s) \quad (23)$$

2.3 The Arbitrarily Damped Case

In the case of arbitrary damping, the matrix C_d is not diagonalized by the undamped mode shapes, and so the problem may not be uncoupled. Again, consider the dynamic equilibrium problem shown in Equation (1). This relation can be written as the following system of equations

$$\begin{bmatrix} C_d & M \\ M & 0 \end{bmatrix} \begin{Bmatrix} \dot{q} \\ \ddot{q} \end{Bmatrix} + \begin{bmatrix} K & 0 \\ 0 & -M \end{bmatrix} \begin{Bmatrix} q \\ \dot{q} \end{Bmatrix} = \begin{Bmatrix} I \\ 0 \end{Bmatrix} f(t) \quad (24)$$

which can be expressed as

$$E\dot{x} + Fx = Q \cdot f(t) \quad (25)$$

Considering the unloaded case,

$$E\dot{x} + Fx = 0 \quad (26)$$

the solution takes the form

$$x = \theta e^{\lambda t} \quad (27)$$

Substituting the solution into Equation (26) gives

$$(E\lambda + F)\theta e^{\lambda t} = 0 \quad (28)$$

As in the undamped derivation, the exponential term cannot equal zero, and so it is clear that

$$(E\lambda + F)\theta = 0 \quad (29)$$

where solution vectors θ are the complex eigenvectors of the system and the corresponding λ values are the complex eigenvalues. It is simple to show that

these results come in conjugate pairs, as the total number of them is twice the order of the system.

Again, if the solutions for two different modes are examined, one has

$$E\theta_j\lambda_j = -F\theta_j \quad (30)$$

$$E\theta_k\lambda_k = -F\theta_k \quad (31)$$

Proceeding in the same manner as the undamped case, it is easy to prove that when $j \neq k$,

$$\theta_k E \theta_j = 0 \quad (32)$$

$$\theta_j F \theta_k = 0 \quad (33)$$

Therefore, the complex eigenvectors, Θ , diagonalize the E and F matrices, and one can write

$$\Theta^T E \Theta = d_E \quad (34)$$

$$\Theta^T F \Theta = d_F \quad (35)$$

At this point it is useful to consider the form of the complex eigenvector, θ_j , remembering that its length is equal to twice the order of the system. If one partitions the eigenvector into two parts and calls the top half the complex mode shape, ψ_j , the bottom half of the vector, R_j , can be solved for by substitution into Equation (29)

$$\begin{bmatrix} C_d & M \\ M & 0 \end{bmatrix} \begin{Bmatrix} \psi_j \\ R_j \end{Bmatrix} \lambda_j + \begin{bmatrix} K & 0 \\ 0 & -M \end{bmatrix} \begin{Bmatrix} \psi_j \\ R_j \end{Bmatrix} = \begin{Bmatrix} 0 \\ 0 \end{Bmatrix} \quad (36)$$

Solving the second equation in this system gives

$$M\psi_j\lambda_j = MR_j \quad (37)$$

and so

$$\psi_j\lambda_j = R_j \quad (38)$$

Therefore

$$\theta_j = \begin{Bmatrix} \psi_j \\ \psi_j\lambda_j \end{Bmatrix} \quad (39)$$

and more generally

$$\Theta = \begin{Bmatrix} \Psi \\ \Psi\Lambda \end{Bmatrix} \quad (40)$$

where Λ is a diagonal matrix containing the complex eigenvalues.

With this relationship in mind, one can investigate the normalization of the modes such that $\Theta^T E \Theta$ is not only diagonal, but equal to the identity.

$$\Theta^T E \Theta = [\Psi^T \quad \Lambda^T \Psi^T] \begin{bmatrix} C_d & M \\ M & 0 \end{bmatrix} \begin{Bmatrix} \Psi \\ \Psi\Lambda \end{Bmatrix} = I \quad (41)$$

Multiplying gives

$$\Psi^T C_d \Psi + \Lambda^T \Psi^T M \Psi + \Psi^T M \Psi \Lambda = I \quad (42)$$

Premultiplication of Equation (29) by Θ^T shows that when $\Theta^T E \Theta = I$,

$$\lambda + \Theta^T F \Theta = 0 \quad (43)$$

and so, considering all the solutions, one has

$$\Theta^T F \Theta = -\Lambda \quad (44)$$

Performing this multiplication gives

$$\Theta^T F \Theta = [\Psi^T \quad \Lambda^T \Psi^T] \begin{bmatrix} K & 0 \\ 0 & -M \end{bmatrix} \begin{bmatrix} \Psi \\ \Psi \Lambda \end{bmatrix} = -\Lambda \quad (45)$$

which is carried out to obtain

$$\Psi^T K \Psi - \Lambda^T \Psi^T M \Psi \Lambda = -\Lambda \quad (46)$$

Therefore, Equations (42) and (46) describe the properties of the desired normalization for complex modes. Examining only the diagonal from Equation (42) shows that for proper normalization,

$$\psi_j^T C_d \psi_j + 2\lambda_j \psi_j^T M \psi_j = 1 \quad (47)$$

Due to the different normalization properties of the classically damped (real) and arbitrarily damped (complex) mode shapes, the expressions for calculating the Receptance are different. While the transfer matrix in the classically damped case is generated as in Equation (22), the expression in the case of complex modes is as derived as follows.

Rearranging the equilibrium equation in Equation (25) and premultiplying by E^{-1} gives

$$\dot{x} = -E^{-1} F x + E^{-1} Q \cdot f(t) \quad (48)$$

which can be written as

$$\dot{x} = A x + B \cdot f(t) \quad (49)$$

From the previous definitions, it is clear that the eigenvectors and eigenvalues of A are θ and λ from Equation (29), and so

$$A\theta = \theta\lambda \quad (50)$$

Considering all solutions and postmultiplying by θ^{-1} , one has

$$A = \theta\Lambda\theta^{-1} \quad (51)$$

which can be substituted into Equation (49) to give

$$\dot{x} = \theta\Lambda\theta^{-1}x + B \cdot f(t) \quad (52)$$

Premultiplying by θ^{-1} and making the substitution $Z = \theta^{-1}x$ yields

$$\dot{Z} = \Lambda Z + \theta^{-1}B \cdot f(t) \quad (53)$$

Taking a Laplace transform and ignoring initial conditions, one gets

$$Z(s) \cdot s = \Lambda Z(s) + \theta^{-1}B \cdot f(s) \quad (54)$$

which can be rearranged to solve for $Z(s)$

$$Z(s) = [I \cdot s - \Lambda]^{-1} \theta^{-1}B \cdot f(s) \quad (55)$$

Remembering the substitution of $Z = \theta^{-1}x$, one can write

$$x(s) = \theta [I \cdot s - \Lambda]^{-1} \theta^{-1}B \cdot f(s) \quad (56)$$

Recalling the forms of $x(s)$ and θ from Equations (24) and (40), it is clear that

$$q(s) = \Psi [I \cdot s - \Lambda]^{-1} \theta^{-1}B \cdot f(s) \quad (57)$$

and so the Receptance, $G(s)$, is defined as

$$G(s) = \Psi[I \cdot s - \Lambda]^{-1} \Theta^{-1} B \quad (58)$$

Since the central matrix being inverted is diagonal, it follows that one can write the following equation if the matrix T is also diagonal.

$$G(s) = \Psi T [I \cdot s - \Lambda]^{-1} T^{-1} \Theta^{-1} B \quad (59)$$

The Receptance is known to be symmetric, and so it is also equal to the transpose of this equation, namely

$$G(s) = B^T \Theta^{-T} T^{-T} [I \cdot s - \Lambda]^{-1} T^T \Psi^T \quad (60)$$

This allows one, after inspection, to write

$$G(s) = \Psi T [I \cdot s - \Lambda]^{-1} T^T \Psi^T \quad (61)$$

Since T is diagonal, the matrices T and T^T can be multiplied and represented by a new diagonal matrix ρ . Making this notation change and writing Equation (61) as a sum gives

$$G(s) = \sum_{j=1}^{2N} \frac{\psi_j \psi_j^T \rho_j}{s - \lambda_j} \quad (62)$$

It is not derived here, but it turns out that the ρ_j term = 1 when the modes are normalized such that Equations (42) and (46) are true.

CHAPTER 3 – MASS PERTURBATION THEORY

3.1 Introduction

In this chapter, a set of derivations are presented for various mass perturbation techniques. Three previously tested methods are explained – the Parloo method (Section 3.2), the Brincker method (Section 3.3), and the Bernal projection method (Section 3.4). Each of these techniques operates under the assumption of classical damping. In Section 3.5, a newer technique, derived for the case of arbitrary damping, is outlined. This technique is called the Receptance method. The characteristics of the methods are summarized and compared in Section 3.6. Finally, Section 3.7 includes a short example illustrating the relationship between the undamped and complex mode normalizations.

3.2 Parloo Expression

The idea of mass perturbation for mode normalization was first proposed by Parloo [3]. A derivation of the original expression is now presented.

The mass of a system, M , may be represented by

$$M = M_0 + \beta M_1 \quad (63)$$

where M_0 is the mass before a perturbation, M_1 is a matrix expressing the distribution of added masses, and β gives the magnitude of the perturbation. The undamped eigenvalue problem for a system with such a mass is written as

$$K\phi_{1,j} = (M_0 + \beta M_1)\phi_{1,j}\lambda_{1,j} \quad (64)$$

where j denotes the particular mode number. The mode shapes and poles of the perturbed system are represented by $\phi_{1,j}$ and $\lambda_{1,j}$, respectively. This notation will be used throughout this section, with “0” denoting the unperturbed state and “1” referring to the condition with a mass change.

If one takes a derivative of Equation (64) with respect to the perturbation magnitude, β , the following is obtained, with the subscript j removed for simplification.

$$K \frac{d\phi_1}{d\beta} = (M_0 + \beta M_1) \phi_1 \frac{d\lambda_1}{d\beta} + (M_0 + \beta M_1) \lambda_1 \frac{d\phi_1}{d\beta} + M_1 \phi_1 \lambda_1 \quad (65)$$

Rearranging and premultiplying by ϕ_1^T yields

$$\phi_1^T [K - (M_0 + \beta M_1) \lambda_1] \frac{d\phi_1}{d\beta} = \phi_1^T (M_0 + \beta M_1) \phi_1 \frac{d\lambda_1}{d\beta} + \phi_1^T M_1 \phi_1 \lambda_1 \quad (66)$$

Remembering Equation (64), it is clear that the left side of Equation (66) is equal to zero. Evaluating the derivative at $\beta=0$, where $\phi_1 = \phi_0$, and rearranging gives

$$\frac{d\lambda}{d\beta}_{\beta=0} = \frac{-\phi_0^T M_1 \phi_0 \lambda_0}{\phi_0^T M_0 \phi_0} \quad (67)$$

Equation (67) is valid for an arbitrary mode scaling. If α is the scaling factor which gives a mass normalized mode, $\bar{\phi}$, such that $\bar{\phi}_{0,j} = \alpha_j \phi_{0,j}$ and $\bar{\phi}_0^T M_0 \bar{\phi}_0 = 1$, then Equation (67) becomes

$$\frac{d\lambda}{d\beta}_{\beta=0} = -\alpha^2 \phi_0^T M_1 \phi_0 \lambda_0 \quad (68)$$

Approximating the derivative with a forward difference and solving for α^2 gives the Parloo equation.

$$\alpha^2 \cong \frac{(\lambda_0 - \lambda_1)}{\lambda_0 \phi_0^T \beta M_1 \phi_0} \quad (69)$$

The accuracy of this equation relies purely on the estimation of the derivative of the eigenvalue. If this quantity can be obtained exactly, the results of the Parloo equation are exact. Accurate estimation of the derivative depends on balancing two competing factors. First, in any experimental determination of modal parameters, there will be measurement error. Therefore, one would like the shift in frequency due to the added mass to be large in comparison to the measurement error. The other factor to consider, however, is the accuracy of the forward difference approximation. If the derivative of the eigenvalue with respect to an added mass is constant, the forward difference will provide a reliable answer in all cases. On the other hand, when the change in an eigenvalue is nonlinear, large shifts in frequency may provide a poor approximation of the derivative at $\beta = 0$. These contradictory factors may lead to a case where finding an accurate estimation of the derivative is difficult.

3.3 Brincker and Andersen Expression

In order to circumvent the difficulty in accurately estimating the derivative of the eigenvalues, an expression was derived by Brincker and Andersen based on a finite change in mass [4]. Looking at the undamped eigenvalue problem of the system in both the original and perturbed states, again with the subscript j removed for simplicity, one has

$$K \phi_0 = M_0 \phi_0 \lambda_0 \quad (70)$$

$$K \phi_1 = (M_0 + \beta M_1) \phi_1 \lambda_1 \quad (71)$$

Subtracting Equation (70) and (71) gives

$$M_0(\phi_0 \lambda_0 - \phi_1 \lambda_1) = \beta M_1 \phi_1 \lambda_1 + K(\phi_0 - \phi_1) \quad (72)$$

If the perturbed mode, ϕ_1 , is expressed as $(\phi_0 + \Delta\phi)$, then premultiplied by ϕ_0^T gives

$$\phi_0^T M_0 [\phi_0 \lambda_0 - (\phi_0 + \Delta\phi) \lambda_1] = \phi_0^T \beta M_1 (\phi_0 + \Delta\phi) \lambda_1 + \phi_0^T K [\phi_0 - (\phi_0 + \Delta\phi)] \quad (73)$$

This equation is exact for an arbitrary scaling of the mode shape. If α is the scaling factor that will give a mass normalized mode, $\bar{\phi}$, such that $\bar{\phi}_{0,j} = \alpha_j \phi_{0,j}$ and $\bar{\phi}_0^T M_0 \bar{\phi}_0 = 1$, then one has

$$\lambda_0 - \lambda_1 - \alpha \phi_0^T M_0 (\Delta\phi) \lambda_1 = \alpha \phi_0^T \beta M_1 (\alpha \phi_0 + \Delta\phi) \lambda_1 - \alpha \phi_0^T K (\Delta\phi) \quad (74)$$

Bringing the last term on the right side to the left side, one can express λ_1 as $(\lambda_0 + \Delta\lambda)$ and group terms to arrive at

$$\lambda_0 - \lambda_1 - \alpha \phi_0^T [M_0 (\lambda_0 + \Delta\lambda) - K] \Delta\phi = \alpha \phi_0^T \beta M_1 (\alpha \phi_0 + \Delta\phi) \lambda_1 \quad (75)$$

It is clear from the eigenvalue solution that $\phi_0^T (M_0 \lambda_0 - K)$ is equal to zero, and so one can rearrange to have

$$\lambda_0 - \lambda_1 = \alpha^2 \phi_0^T \beta M_1 \phi_0 \lambda_1 + \alpha \phi_0^T \beta M_1 (\Delta\phi) \lambda_1 + \alpha \phi_0^T M_0 (\Delta\lambda) (\Delta\phi) \quad (76)$$

If it is assumed that the mode shapes do not change due to the perturbation ($\Delta\phi = 0$), the last two terms are zero, and what remains is

$$(\lambda_0 - \lambda_1) \cong \alpha^2 \phi_0^T \beta M_1 \phi_0 \lambda_1 \quad (77)$$

which can be rearranged to arrive at the Brincker equation

$$\alpha^2 \cong \frac{(\lambda_0 - \lambda_1)}{\lambda_1 \phi_0^T \beta M_1 \phi_0} \quad (78)$$

As stated earlier, this formula does not rely on computing an approximation for the derivative of a system's eigenvalues. The only assumption that it rests on is that the mode shapes are unchanged by the mass perturbation. This condition will hold if the added mass configuration is proportional to the mass of the original system. This cannot be expected to occur in practical applications (although distributing multiple masses is recommended).

It should also be noted that the Brincker expression is identical to the Parloo expression with one small exception – the use of the eigenvalue from the perturbed state in the denominator rather than the original state. Since the difference in frequency due to the mass change should not be more than a few percent, these two equations can be expected to give relatively similar results.

3.4 Bernal Projection Expression

A suggested improvement to the Brincker equation has stemmed from removing the assumption of unchanging mode shapes. Instead, Bernal proposed that mode shapes in the perturbed state be expressed in the basis of the original modes [5]. For a particular mode, this can be written as

$$\phi_{1,j} = \Phi_0 q_j \quad (79)$$

where Φ_0 is the full set of arbitrarily scaled system modes. The variable q_j represents a coefficient vector. Substituting into the perturbed undamped eigenvalue problem, Equation (71), gives

$$K\Phi_0 q_j = (M_0 + \beta M_1)\Phi_0 q_j \lambda_{1,j} \quad (80)$$

Premultiplying by Φ_0^T , one gets

$$\Phi_0^T K \Phi_0 q_j = \Phi_0^T (M_0 + \beta M_1) \Phi_0 q_j \lambda_{1,j} \quad (81)$$

which can be rearranged to yield

$$\Phi_0^T K \Phi_0 q_j - \Phi_0^T M_0 \Phi_0 q_j \lambda_{1,j} = \Phi_0^T \beta M_1 \Phi_0 q_j \lambda_{1,j} \quad (82)$$

Again, assuming α is the modal scaling factor that mass normalizes the modes ($\bar{\phi}_{0,j} = \alpha_j \phi_{0,j}$), simplifications may be made, namely that $\bar{\Phi}_0^T M_0 \bar{\Phi}_0 = I$ and $\bar{\Phi}_0^T K \bar{\Phi}_0 = \Lambda_0$, where Λ_0 is a diagonal matrix containing the eigenvalues of the unperturbed system. In addition, one may make the substitution of Equation (79) on the right side to get

$$(\Lambda_0 - I\lambda_{1,j})\bar{q}_j = \hat{\alpha} \Phi_0^T \beta M_1 \phi_{1,j} \lambda_{1,j} \quad (83)$$

In this equation $\hat{\alpha}$ represents a diagonal matrix containing the scaling factors. The values for \bar{q} in this equation correspond to the condition of mass normalized modes ($\phi_{1,j} = \bar{\phi}_0 \bar{q}_j$), which was assumed prior to Equation (83). Remembering Equation (79), one has

$$\phi_0 q_j = \bar{\phi}_0 \bar{q}_j \quad (84)$$

If the mass normalized modes take the form previously assumed ($\bar{\phi}_{0,j} = \alpha_j \phi_{0,j}$), then

$$\bar{q}_j = \hat{\alpha}^{-1} q_j \quad (85)$$

Substituting into Equation (83) and premultiplying by $\hat{\alpha}^{-1}$ gives

$$\hat{\alpha}^{-1}(\Lambda_0 - I\lambda_{1,j})\hat{\alpha}^{-1}q_j = \Phi_0^T \beta M_1 \phi_{1,j} \lambda_{1,j} \quad (86)$$

Because the matrices on the left hand side are diagonal, this can be rearranged to give

$$\hat{\alpha}^{-2}(\Lambda_0 - I\lambda_{1,j})q_j = \Phi_0^T \beta M_1 \phi_{1,j} \lambda_{1,j} \quad (87)$$

Note that this equation differs from the Parloo and Brincker equations in that each mode considered provides scaling factors for all other modes. When perfect information is available, it does not matter how one handles the redundant results. However, in the presence of noise, the most accurate estimate for each mode is seen when the most similar vector of Φ_0 is used in the calculation. Simplifying Equation (87) for this method of application gives the Bernal projection formula for a particular mode

$$\alpha^2 \cong \frac{(\lambda_0 - \lambda_1)\kappa}{\lambda_1 \phi_0^T \beta M_1 \phi_1} \quad (88)$$

where κ is the corresponding value of q_j to the mode being normalized.

The projection method gives exact results when the coefficient κ is correct. If all the modes of the system are available, the equation will be exact since the matrix of the original modes, Φ_0 , will be full rank and provide for perfect projection. In addition, there are a few cases where the results will be exact even with a truncated mode set.

First, if the mass perturbation is proportional to the original mass, the mode shapes do not change. In this case, q_j in Equation (79) is the identity, and κ for each particular mode is equal to 1. It is interesting to note that in this situation, the Bernal projection formula is identical to the Brincker equation, and both are exact.

Second, the method is also exact if the mass of the system is proportional to the identity and all coordinates are measured. Since the modes are orthonormal in this case, the value of q_j for a particular mode is independent of the other modes, and the truncated mode set causes no error.

Finally, the method is exact if the perturbed modes are in the span of the unperturbed modes such that full projection is possible in Equation (79). It is important to note that this condition refers to the “true” mode shapes of the system, not simply measured mode shapes from experiment, which represent only a partial set of the system’s degrees of freedom.

3.5 Receptance Method

With the existing normalization techniques derived above, it is important to reiterate that all three methods (Parloo, Brincker, and Bernal projection) are derived from an undamped eigenvalue problem. If a system is classically damped, it is not difficult to compute the undamped results from the damped solution. Although this assumption of classical damping does not introduce significant error in many applications, it will never be true in a practical case. In some situations, there may be significant complexity in the mode shapes due to nonclassical damping, which would complicate the application of the above techniques. Therefore, a method has been proposed that can be applied to an arbitrarily damped system and does not require real mode shapes [6].

Begin with the dynamic equilibrium equation for a viscously damped linear time invariant system, namely

$$M\ddot{q}(t) + C_d\dot{q}(t) + Kq(t) = f(t) \quad (89)$$

where M , C_d , and K are the mass, damping, and stiffness matrices, respectively, for an N degree of freedom system, and $f(t)$ are the applied loads. Taking a Laplace transform and assuming zero initial conditions gives

$$[Ms^2 + C_d s + K]y(s) = f(s) \quad (90)$$

Values of s for which the matrix on the left side of Equation (90) loses rank are the poles, or complex eigenvalues, λ , and the vectors associated with the null

space are the complex mode shapes, ψ . It is important to point out that these eigenvalues should not be compared directly to the eigenvalues of the undamped system. While the eigenvalues from the undamped problem represent the square of the undamped frequencies, the complex eigenvalues from the damped equations come in conjugate pairs and take the form

$$\lambda_j = -\omega_j \zeta_j \pm \omega_j \sqrt{1 - \zeta_j^2} i \quad (91)$$

where ω_j is the undamped frequency and ζ_j is the percent of critical damping for mode j . The imaginary part of this expression is referred to as the damped frequency, ω_D .

For any values of s other than the eigenvalues, the matrix on the left side of Equation (90) is invertible. Remembering Equation (23), it is clear that this inverse is equal to the Receptance, as it provides the linear map between input and output in the Laplace domain.

As proven in a previous section, the Receptance can be expressed as a sum in terms of the poles and complex mode shapes. Expressing the constant in the numerator of Equation (62) as an α^2 for consistency gives

$$G(s) = \sum_{j=1}^{2N} \frac{\psi_j \psi_j^T \alpha_j^2}{s - \lambda_j} \quad (92)$$

When the modes are normalized such that Equations (42) and (46) are true, the scaling factors are equal to 1.

If the damped eigenvalue problem in the perturbed condition is examined, one has

$$[(M_0 + \beta M_1)\lambda_{1,j}^2 + C_d\lambda_{1,j} + K]\psi_{1,j} = 0 \quad (93)$$

which can be rearranged to give

$$[M_0\lambda_{1,j}^2 + C_d\lambda_{1,j} + K]^{-1}\beta M_1\lambda_{1,j}^2\psi_{1,j} = -\psi_{1,j} \quad (94)$$

Inspection of Equation (94) shows that the inverted matrix is simply the Receptance of the original system evaluated at $s = \lambda_{1,j}$, and so

$$\sum_{i=1}^{2N} \left(\frac{\psi_{0,i}\psi_{0,i}^T\alpha_i^2}{\lambda_{1,j} - \lambda_{0,i}} \right) \beta M_1\lambda_{1,j}^2\psi_{1,j} = -\psi_{1,j} \quad (95)$$

which can be rearranged to give

$$\sum_{i=1}^{2N} \frac{\psi_{0,i}(\psi_{0,i}^T\beta M_1\psi_{1,j})\lambda_{1,j}^2}{\lambda_{0,i} - \lambda_{1,j}}\alpha_i^2 = \psi_{1,j} \quad (96)$$

Equation (96) represents a system of m equations, where m is the number of measurements in the mode shapes. The equation can be evaluated for each perturbed mode to produce $(m \times j)$ equations, where j is the number of modes being normalized. If j is equal to $2N$, where N is the true order of the system, then the result is exact. Otherwise, there will be error due to truncation, since the result for each mode relies in part on all the other modes of the system. However, it is clear from the denominator of the expression that the result will be dominated by the perturbed mode being considered and those near it.

Evaluating Equation (96) for the available modes will yield an overdetermined system of equations taking the well known form $Ax=b$, where the unknowns are the j modal scaling factors. A convenient way for formulating this system of equations is now presented.

The set of equations can be written as

$$Q\bar{\alpha}^2 = \text{vec}(\Psi_1) + \varepsilon \quad (97)$$

where vec is the stacking operator, used to form a column containing the perturbed modes. The matrix Q is generated as

$$Q = \begin{bmatrix} \Psi_0 \chi_1 \\ \Psi_0 \chi_2 \\ \vdots \\ \Psi_0 \chi_n \end{bmatrix} \quad (98)$$

where $\chi_j = \text{diag}(c_j^1, c_j^2, \dots, c_j^n)$ and

$$c_j^k = \left(\frac{\lambda_{1,j}^2}{\lambda_{0,k} - \lambda_{1,j}} \right) \psi_{0,k}^T \beta M_1 \psi_{1,j} \quad (99)$$

Formulating the problem in this way allows one to solve for the least squares solution in this system of equations by way of the pseudoinverse. When the set of identified modes is incomplete, the expression is not exact, but an approximation

$$\bar{\alpha}^2 \cong Q^{-+} \cdot \text{vec}(\Psi_1) \quad (100)$$

where $\bar{\alpha}^2$ is a column vector containing the square of the modal scaling factors for each mode.

3.6 Summary of Methods

Having derived the four equations compared in this thesis, a summary is now presented.

- Parloo's method is based on taking the derivative of the undamped eigenvalue equation with respect to a mass perturbation. Its error is due to a forward difference approximation for the derivative of the eigenvalue. If this derivative can be computed exactly, Equation (69) is exact.
- Brincker's expression is derived by considering a finite mass change to the system. It is based on the assumption that the mode shapes do not change due to the perturbation. When the added mass configuration is proportional to the original mass of the system, this assumption is warranted, and Equation (78) is exact.
- The Bernal projection formula, Equation (88), is based on knowing the diagonal of the matrix that, when multiplied by the original modes, gives the perturbed ones. The needed coefficients can be computed exactly: a) when the modes do not change (since they are then unity) – in which case the formula coincides with that of Brincker and Andersen, b) when the mass matrix is proportional to the identity and all coordinates are measured because the modal matrix is orthonormal and c) whenever the identified basis has the same span in the original and perturbed states.
- The new method based on the Receptance can be used with an arbitrarily damped system (complex modes). It generates an overdetermined system of equations, which allows the modal scaling factors to be solved for with a least-squares solution. When there is no modal truncation, Equations (98), (99), and (100) provide an exact answer.

It is worth repeating that the first three methods (Parloo, Brincker, and Bernal projection) assume classical damping and provide mass normalization of modes. For this particular normalization, the modes are purely real and $\Phi^T M \Phi = I$.

On the other hand, the Receptance method does not assume classical damping and the resulting mode normalization is different. Instead of mass normalization, the modes, complex in this case, are scaled such that Equations (42) and (46) are satisfied and the Receptance can be calculated using Equation (62) with the scaling factor ρ_j equal to 1.

So, the modes normalized via the Receptance method cannot be directly compared to those from the other techniques. If the system is classically damped, however, the modes normalized according to Equations (42) and (46) can be transformed to the related mass normalized modes by multiplication with $\sqrt{2\omega_D i}$, where ω_D is the damped frequency, or the imaginary part of the complex eigenvalue. This simple calculation allows the mode shapes from all four methods to be compared in the real domain (provided that we accept the normal mode model).

3.7 Normalization Example

To illustrate by example the relationship between the mass normalized modes of the classically damped methods and the complex modes of the Receptance method, consider a system with three degrees of freedom having the following mass and stiffness matrices.

$$M = \begin{bmatrix} 1 & 0 & 0 \\ 0 & 2 & 0 \\ 0 & 0 & 3 \end{bmatrix} \quad K = \begin{bmatrix} 200 & -100 & 0 \\ -100 & 200 & -100 \\ 0 & -100 & 100 \end{bmatrix}$$

If the system is classically damped, with a 2% damping ratio on each mode, the damping matrix is

$$C_d = \begin{bmatrix} 0.5508 & -0.1799 & -0.0363 \\ -0.1799 & 0.7175 & -0.3011 \\ -0.0363 & -0.3011 & 0.5831 \end{bmatrix}$$

One can find the solution to the undamped eigenvalue problem by computing the eigenvectors of $M^{-1}K$. When these eigenvectors, Φ , are normalized such that $\Phi^T M \Phi = I$, the result is

$$\Phi = \begin{bmatrix} 0.1904 & -0.4453 & -0.8749 \\ 0.3655 & -0.5036 & 0.3358 \\ 0.4818 & 0.3133 & -0.0546 \end{bmatrix}$$

and the corresponding undamped frequencies are 2.8364, 9.3222, and 15.4397 radians per second.

The complex eigenvectors can be found by formulating the matrix A as defined in Equations (48) and (49).

$$A = \begin{bmatrix} 0 & I \\ -M^{-1}K & -M^{-1}C_d \end{bmatrix}$$

One can find the six eigenvectors and eigenvalues of this matrix and consider only one of each conjugate pair. Also recall that the top half of these eigenvectors are the complex mode shapes of the system, Ψ . When these vectors are normalized such that Equations (42) and (46) are true, the result is

$$\Psi = \begin{bmatrix} 0.0565 - 0.0565i & 0.0729 - 0.0729i & 0.1113 - 0.1113i \\ 0.1085 - 0.1085i & 0.0825 - 0.0825i & -0.0427 + 0.0427i \\ 0.1431 - 0.1431i & -0.0513 + 0.0513i & 0.0069 - 0.0069i \end{bmatrix}$$

and the complex eigenvalues are $-0.0567 + 2.8358i$, $-0.1864 + 9.3203i$, and $-0.3088 + 15.4366i$.

To find the relation between these different normalizations, one can divide the undamped modes by the complex modes. If the result (a constant) for each

mode is squared and divided by $2i$, then one has the imaginary part of the complex eigenvalue (or the damped frequency), as would be expected if

$$\phi_j = \sqrt{2\omega_{D,j}} i \psi_j.$$

CHAPTER 4 - EXPERIMENTAL CAMPAIGN

4.1 Introduction

In this chapter, the computer modeling and experimental testing used to compare the mass modification methods is outlined. In Section 4.2, the experimental test setup and identification procedure is explained. Section 4.3 presents the results of a forced vibration test, done for the purposes of obtaining correctly normalized modes. Section 4.4 describes the preliminary modeling and testing conducted to ensure proper application of the mass perturbation methods. Finally, Section 4.5 details the output-only testing results and the comparative success of the various mode normalization methods.

4.2 Test Setup and Identification Procedure

In order to compare the effectiveness of the various mass modification techniques, a series of tests was conducted on an aluminum plate. The 1.90 kg plate (48.5 cm x 30.5 cm x 0.6 cm) was suspended using two elastic bungee cords to simulate a free-free boundary condition. During the tests, nine accelerometers located along the centerlines provided dynamic response data in the direction perpendicular to the plane of the plate.

The two types of tests conducted are referred to in this thesis as *forced vibration tests* and *operational tests*. The input during forced vibration tests was provided by a shaker. Both the applied force and the acceleration at the shaker location were measured, allowing correctly scaled mode shapes to be obtained. In the operational testing, excitation was provided through a piezoelectric wafer at a location relatively close to the shaker input. In both the forced vibration and operational tests, the excitation was a random white noise signal, and the measured bandwidth was from 0-1280 Hz. The configuration of the accelerometers and excitation locations is shown in Figure 1, a photograph of the

plate. One should note the grid of drilled holes, which were used to securely attach both accelerometers and added masses.

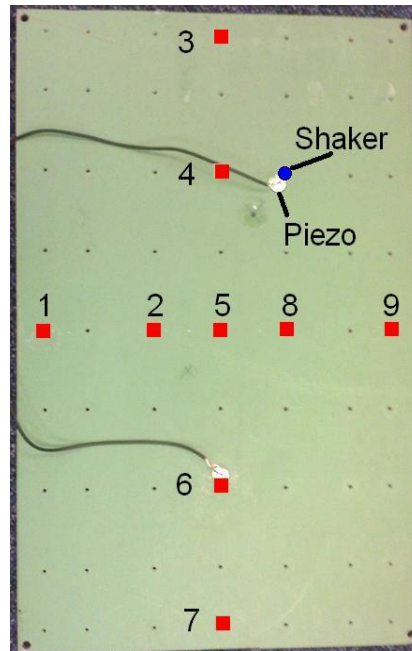


Figure 1: Photograph of plate with accelerometer configuration (red) and excitation location

The vibration data was recorded and analyzed to obtain modal models of the system. In the case of forced vibration tests, frequency response functions (FRFs) were calculated using the measured acceleration outputs and force input. Acceleration time histories from operational testing were used to calculate cross power functions. The FRFs and cross power functions were then analyzed using a Polymax Modal Analysis toolbox. This tool fits the given data to models of varying order and presents the user with a stabilization diagram, shown in Figure 2.

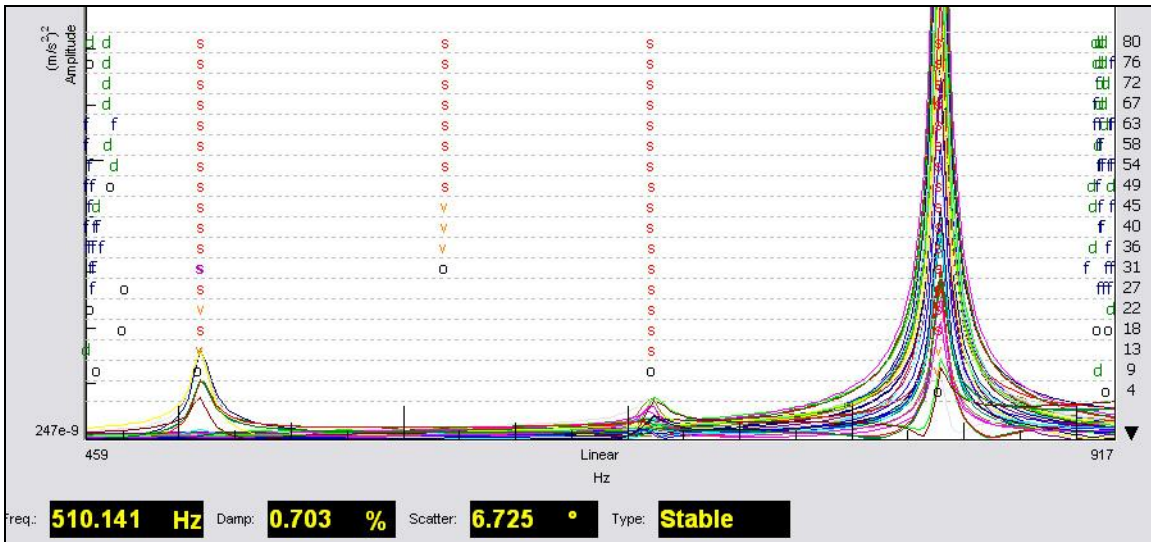


Figure 2: Stabilization diagram for pole selection in LMS Test.Lab software

At this point, poles which are stable with respect to model order are selected. With this procedure, the desired modal parameters (mode shapes, frequencies, and damping values) were obtained.

4.3 Forced Vibration Test Results and Verification

Comparing the results of the different mass modification expressions requires that correctly scaled mode shapes be known. For this purpose, a shaker test was performed with a measured input. The sampling frequency was 2560 Hz, and the duration of the test was 6.4 seconds. A picture of the forced vibration test setup is shown in Figure 3.

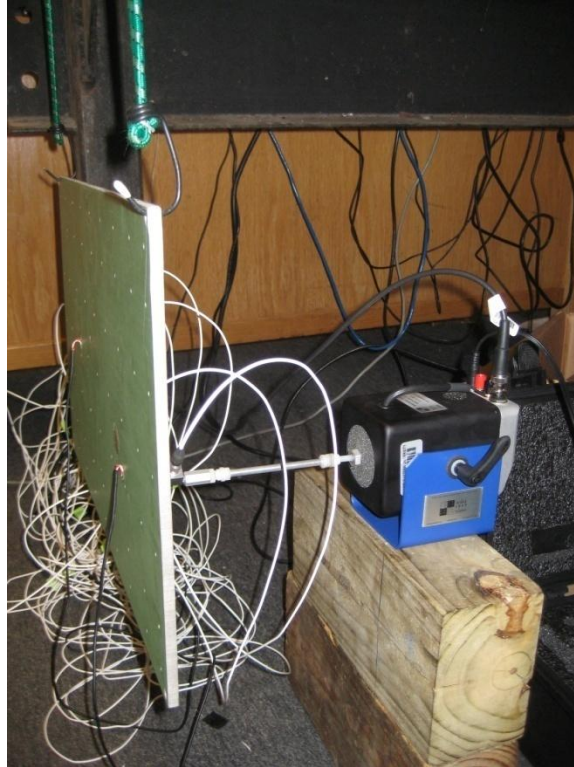


Figure 3: Shaker setup for forced vibration test

After processing the results from this test, three modes were selected as the test set for this study. The modes were chosen because they were sufficiently spaced to allow for easy application of the methods. Also, they were readily identifiable under the particular sensor and shaker configuration being used. The frequency and damping ratio information for the three selected modes can be found in Table 1.

Table 1: Test mode set selected from forced vibration data

Mode	f (Hz)	ζ (%)
1	508.84	0.78
2	709.69	0.48
3	837.06	0.33

As stated in a previous section, properly normalized mode shapes can be used to calculate the Receptance - to and from - any measured location. As shown in Figure 4, the Receptance computed using the selected modes provides an

accurate estimation of the experimentally measured FRF over the relevant bandwidth.

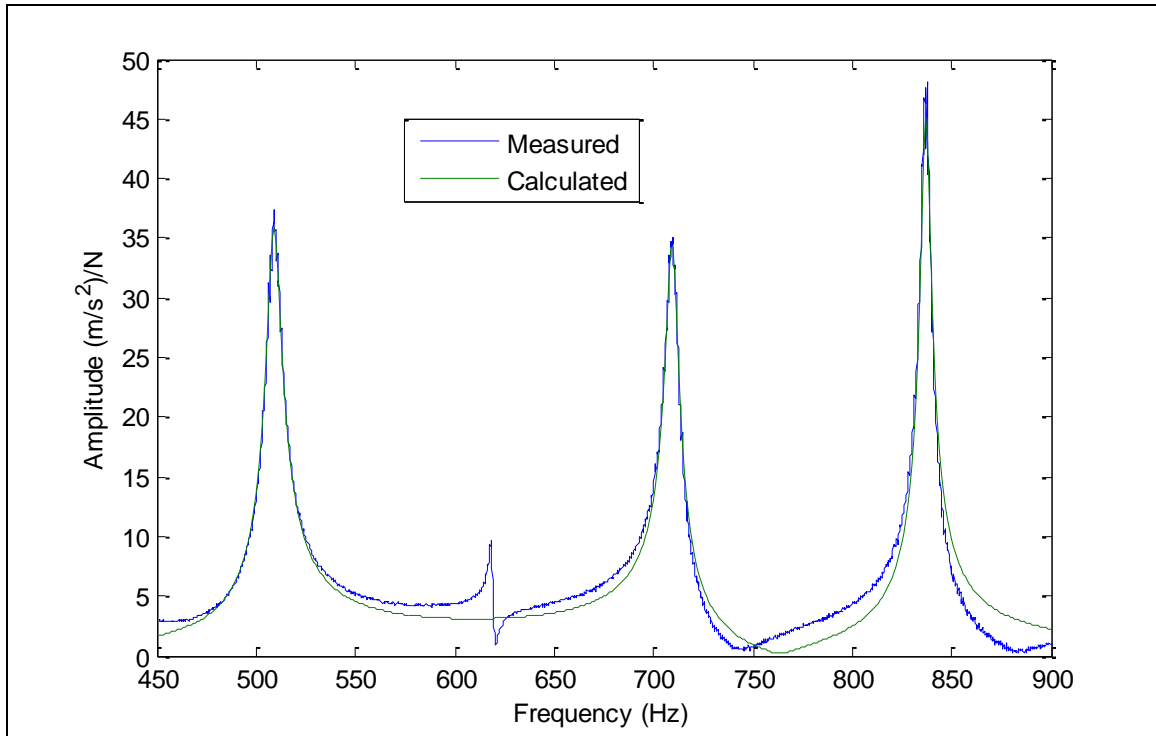


Figure 4: Frequency response function comparison - measured directly vs. generated from identification results (shaker to point 3)

For the purposes of this thesis, the mode shapes normalized using the shaker test will be considered the “true” shapes. They represent the results one gets from a standard forced vibration test with a measured input. The mass modification algorithms will be compared based on how well they can reproduce these results through multiple output-only tests. Perfect normalization through mass modification would equate to a full recovery of the information lost due to output-only testing.

4.4 Preliminary Studies

Before proceeding to application of the mass modification techniques, it was necessary to determine how large induced frequency shifts would need to be to

overcome measurement error. As explained in an earlier section, stabilization diagrams were used to obtain a modal model of the system by analyzing the data assuming different model orders. There is a certain variability in the mode frequencies due to the changing order. To quantify this variability, five operational tests were performed on the plate with no masses added. A standard deviation was computed for each mode based on the results from the different tests and selecting different model orders. The results are summarized in Table 2.

Table 2: Summary of Error Margins for Selected Frequencies

	<i>Mode 1</i>	<i>Mode 2</i>	<i>Mode 3</i>
σ (Hz)	0.316	0.207	0.181
10σ (Hz)	3.16	2.070	1.813

It was decided that frequency shifts should be ten times larger than the standard deviation to provide confidence in results. Therefore, 3.16 Hz (the largest value for any of the 3 modes) was chosen as the minimum desired shift.

Aside from examining the error characteristics of the identification methods, it was also worthwhile to investigate predicted frequency shifts based on a model of the plate. This finite element model, created in Abaqus allowed for different mass addition configurations to be investigated without the complication of measurement error. The results of the study are shown in Table 3, which lists the frequency shifts of the three selected modes as a 13.5 g mass was moved to the different sensor locations.

Table 3: Frequency shift results for various mass modifications (Abaqus model)

Added Mass Location	Frequency Shift		
	Mode 1	Mode 2	Mode 3
1	0.01	<u>8.61</u>	2.06
2	0	0.94	<u>5.3</u>
3	1.37	<u>8.15</u>	0.59
4	<u>3.31</u>	0.31	<u>5.48</u>
5	0	<u>3.54</u>	<u>6.17</u>
6	3.02	0.4	<u>3.34</u>
7	1.31	<u>7.96</u>	0.5
8	0	0.86	<u>5.52</u>
9	0	<u>8.64</u>	2.54
4+7	<u>4.73</u>	<u>8.25</u>	<u>3.88</u>

The underlined numbers represent frequency shifts larger than the desired threshold of 3.16 Hz. These particular mass configurations and corresponding modes are, therefore, good candidates for application of the modification techniques, as the resulting shifts should contain acceptably low levels of measurement error.

Although no single mass addition was able to produce the desired shifts in all three modes simultaneously, the model results did allow a multi-mass configuration to be selected. As seen in the last row of Table 3, the addition of 13.5 g masses at sensor locations 4 and 7 generated the required shifts in the three modes.

4.5 Operational Tests and Implementation of Methods

For the operational, or output-only, testing, a piezoelectric wafer actuator was the chosen method of excitation for a number of reasons. First, the mass and stiffness of the actuator are negligible when compared to the plate. This provides a noninvasive input without altering the characteristics of the system being identified. Second, the nature of the applied input is atypical. Whereas the direction and magnitude of the input from a shaker or hammer test is well understood and relatively easy to measure, the force applied by the piezoelectric

wafer is neither. The wafer provides what can be described as a “stretching” force by expanding and contracting on the surface of the plate. This creates a bending effect that does not occur in the direction of a measured degree of freedom. Due to the fact that the input is difficult to characterize, modal testing using piezoelectric wafers as excitations can benefit from the mass change strategy to for mass normalization.

A piezoelectric wafer, pictured in Figure 5 next to a dime to demonstrate size, was glued to the plate in a location similar to the shaker input.

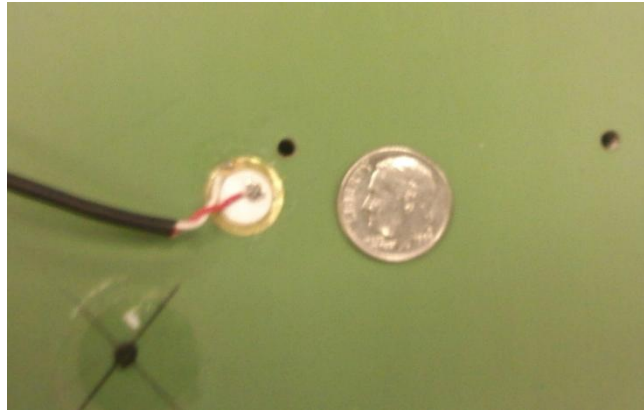


Figure 5: Photograph of piezoelectric wafer actuator glued to plate surface (pictured with dime to show relative size)

A 25 V white noise signal was sent to the wafer. The actual force at the interface between the wafer and the plate, however, is unknown. As with the force vibration test, the sampling rate was 2560 Hz, but in this case the test duration was significantly longer (approximately 13 minutes). This extended duration minimized the effect of measurement noise on the results. The recorded time data from the nine accelerometers was used to compute cross power functions, which were analyzed as described in a previous section. From this analysis, frequencies, damping ratios, and arbitrarily scaled mode shapes were obtained. The results from this test are compared with the output from the shaker test in Table 4.

Table 4: Comparison of forced vibration and operational parameters

Mode	Force Vibration		Output-Only		% Difference		MAC
	f (Hz)	ζ (%)	f (Hz)	ζ (%)	f (Hz)	ζ (%)	
1	508.84	0.78	510.08	0.7	-0.24%	10.26%	0.9994
2	709.69	0.48	710.76	0.58	-0.15%	-20.83%	0.9995
3	837.06	0.33	839.23	0.32	-0.26%	3.03%	0.9997

As the table shows, the frequency results from the operational test were almost identical to those from the forced vibration test, and the MAC numbers showed very good agreement in the mode shapes. As is usually the case, the damping values on each of the modes did not agree quite as well. In this case, the extremely low damping values contributed to the difficulty, since very small absolute differences result in large coefficients of variation.

With accurate mode shapes obtained from the first operational test, the next task was to apply the mass modification techniques to correctly scale the shapes. The mass configurations which were modeled using Abaqus were used to conduct ten different test runs. Table 5 provides a summary of the frequency shifts in each mode under the different added-mass conditions.

Table 5: Frequency shifts for various mass modifications (experimental data)

Added Mass Location	Frequency Shift		
	Mode 1	Mode 2	Mode 3
1	-0.11	<u>11.80</u>	1.95
2	0.16	2.17	<u>5.65</u>
3	1.04	<u>12.10</u>	0.09
4	<u>3.71</u>	1.09	<u>3.20</u>
5	-0.13	<u>5.26</u>	<u>6.22</u>
6	<u>3.67</u>	2.44	<u>3.46</u>
7	0.90	<u>10.57</u>	0.14
8	-0.11	2.56	<u>5.05</u>
9	-0.23	<u>12.81</u>	1.12
4+7	<u>4.80</u>	<u>9.17</u>	<u>4.33</u>

As in Table 3, the underlined values represent frequency shifts which can be considered sufficient for accurate mode shape normalization. The Abaqus model

proved to be a fairly accurate guide for these results, as the pattern of frequency shifts compared favorably to the predicted values. The mass configurations which produced shifts greater than 3 Hz in the model had similar effects on the physical plate.

4.6 Results and Comparison of Methods

At this point in the study, the frequencies, damping ratios, and mode shapes for both the unmodified and modified conditions are known. With all of the required information available, the various mass modification techniques were applied to the cases where frequency shifts were of sufficient magnitude (3.16 Hz). Since the correct mode normalization was known from the forced vibration test, it was simple to calculate what the ideal modal scaling factor would have been for each mode. For the proposed Receptance method, this modal scaling factor was a complex number, which produces a normalization such that Equation (92) can be used to calculate the Receptance. For the other techniques, the scaling factor was a real number, which produces a mass normalized mode shape. In either case, the results from the mass modification techniques can be compared to the ideal modal scaling factor, and a percent error can be calculated. Table 6 summarizes the results of the different techniques with the various added-mass configurations.

Table 6: Comparison of mode normalization methods (% error)

Mass Loc	Mode	Parloo	Brincker	Bernal	Receptance
1	2	-3.67%	-5.42%	-5.52%	7.83%
2	3	4.43%	3.78%	4.47%	4.31%
3	2	-10.32%	-12.23%	-17.88%	-13.88%
4	1	1.55%	0.83%	-0.22%	-0.46%
	3	8.73%	8.38%	7.05%	6.76%
5	2	-15.57%	-16.44%	-13.33%	-7.35%
	3	9.84%	9.16%	6.77%	6.62%
6	1	1.38%	0.67%	-0.52%	-0.50%
	3	7.54%	7.16%	6.30%	5.98%
7	2	-2.65%	-4.20%	-6.51%	-5.27%
8	3	11.33%	10.79%	11.45%	11.39%
9	2	-17.54%	-19.70%	-21.46%	-9.49%
4+7	1	6.93%	6.04%	6.65%	6.19%
	2	5.49%	4.26%	0.75%	-2.03%
	3	2.20%	1.69%	-1.99%	-2.04%
<i>Average</i>		7.28%	7.38%	7.39%	6.01%

Over a series of test runs with ten different mass configurations, the average performance of the Parloo, Brincker, and Bernal projection methods was similar (between 7.2% and 7.4%). The proposed Receptance method, however, did perform markedly better, with an average error of 6.01%. Figure 6 shows the mode shapes normalized with the Receptance method compared to the correctly scaled shapes from the force vibration test. To make the comparison graphically easier, these complex modes were multiplied by $\sqrt{2\omega_D i}$ to produce the corresponding real mass normalized modes. These results are from the multiple-mass test run, where 13.5 g masses were placed at sensor locations 4 and 7. As expected from the modeling, this distributed mass configuration was able to produce large enough shifts to normalize all three modes with one run.

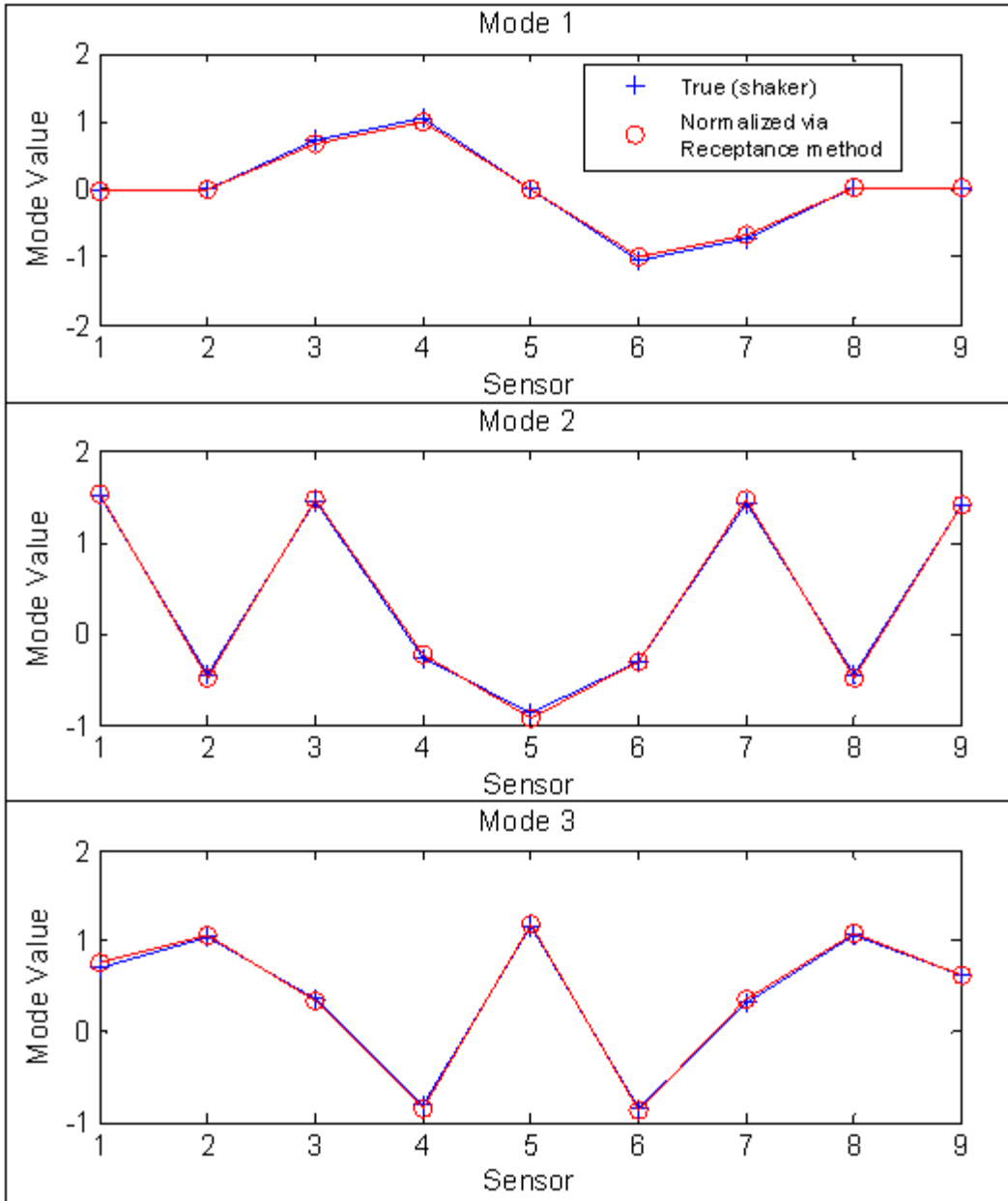


Figure 6: Comparison of shaker modes to modes normalized with Receptance method

From examining Figure 6, it is clear that the results from the forced vibration test can be reasonably replicated with output-only testing through mass modification.

CHAPTER 5 – SUMMARY AND CONCLUSIONS

This thesis presents a summary of the theory of existing techniques to normalize eigenvectors identified from output signals and presents the results of an experimental campaign where these techniques were applied to normalize the eigenvectors of an aluminum plate.

One aspect that was noted in the work is that the need for normalization from mass perturbations may be connected not only to the case of civil structures such as buildings or bridges where the input cannot be measured, but also to other test setups where the input is difficult to characterize. In the case of this experimental program, for example, the piezoelectric wafer actuator provided an extremely cost-effective and noninvasive method of excitation. Effective mass modification techniques allow this convenient source of input to be implemented without suffering the information loss from the lack of a measured excitation force.

There are several conclusions which can be made from the work done in this study.

- The Receptance method can effectively be used to normalize mode shapes from output-only testing. It was possible to properly scale all three considered modes with just one mass perturbation run when multiple masses were used. In this case, the technique was able to recreate the results from a forced-vibration test with an error of less than 7% on all modes.
- When compared to the previously established methods of Parloo, Brincker, and Bernal projection, the new Receptance technique performed favorably. While the other methods provided similar result quality to each other (between 7.2% and 7.4% error over a series of tests), the

Receptance method had an average error of 6.0% for the same set of tests.

- Examining the underlying assumptions for each of the mass normalization methods, it is clear that the Receptance method has a unique advantage in that it does not assume classical damping. In this particular experimental setting, with extremely low damping values, it was unlikely that this difference would result in a significant performance improvement. However, in a system with highly complex modes, where the real modal model does not provide a good approximation, the advantages of the Receptance method should be highlighted.
- A piezoelectric wafer actuator served as a suitable source of excitation for an output-only test. The wafer provided a noninvasive method of input and was able to adequately excite modes in the desired frequency range (500-850 Hz). By using different excitation locations and specifying other bandwidths for the white noise input signal, it is likely that many other modes could be identified with this type of loading.

REFERENCES

1. Brincker R, Ventura CE, Anderson P. Why Output-Only Modal Testing is a Desirable Tool for a Wide Range of Practical Applications. *Proc. of the 21st International Modal Analysis Conference (IMAC XXI)* 2003; Paper 265.
2. Bernal D. Load vectors for damage localization. *Journal of Engineering Mechanics* 2002; **128**(1): 7-14.
3. Parloo E, Verboven P, Guillaume P, Van Overmeire. M. Sensitivity-Based Operational Mode Shape Normalisation. *Mechanical Systems and Signal Processing* 2002; **16**(5): 757-767.
4. Brincker R, Anderson P. A Way of Getting Scaled Mode Shapes in Output Only Modal Testing. *Proc. of the 21st International Modal Conference (IMAC XXI)* 2003; Paper 141.
5. Bernal D. Modal Scaling from Known Mass Perturbations. *Journal of Engineering Mechanics* 2004; **130**(9): 1083-1088.
6. Bernal D. Normalization of Complex Eigenvectors from Mass Perturbation. *Journal of Engineering Mechanics*; (in review).
7. Parloo E, Cauberghe B, Benedettini F, Alaggio R, Guillaume P. Sensitivity-based operational mode shape normalization: Application to a bridge. *Mechanical Systems and Signal Processing* 2005; **19**(1): 43-55.
8. Fernandez P, Reynolds P, Aenlle ML. Experimental Evaluation of Mass Change Approaches for Scaling Factors Estimation. *Proc. of the 28th International Modal Analysis Conference* 2010; Paper 152.

APPENDIX

Relevant Matlab Code

MAIN FILE

```
clear
clc
close all

% map converting sensor locations to geometry in Test.Lab
map=[5 14 28 30 32 34 36 50 59];

% input mass modification information
mm=13.5/1000;%mass in kg (total mass of plate is 1.9 kg
locm=[4 7]; %sensor locations of added mass
M1=[1 1]; %added mass distribution
modsel=[1:3]; %modes to be normalized

%load data and obtain modes
[fic,lamc,f,j]=importTLmodes('test1modes_720',3,9,0); %original
[ficm,lamcm,fm,dum]=importTLmodes('test2modes_720',3,9,0); %perturbed
fdif=f-fm; %compute frequency shifts

%select modes from modsel
fic=fic(:,modsel);
ficm=ficm(:,modsel);
lamc=lamc(modsel);
lamcm=lamcm(modsel);

%repeat data loading for real method
[fir,dum,f,j]=importTLmodes('test1modes_720',3,9,0);
[firm,dum,fm,dum]=importTLmodes('test2modes_720',3,9,0);
fir=fir(:,modsel);
firm=firm(:,modsel);
j=j(modsel);

%calculate omega squared values
lamr=(f(modsel)*2*pi).^2;
lamrm=(fm(modsel)*2*pi).^2;

%load "true" modes from shaker test and correctly normalize
[fit,lamct,ft,jt]=importTLmodes('shakertest1_720',3,10,1);
fit=fit(:,modsel);
lamct=lamct(modsel);
ft=ft(modsel);
jt=jt(modsel);
for aa=1:length(lamc)
    fit(:,aa)=fit(:,aa)/sqrt(fit(8,aa));
end
```

```

%remove measurement from driving point so that sensor locations match
up
fit(8,:)=[];

%implement Receptance method
vec=zeros(9,1);
vec(locm)=.0135;
[kapa1]=normandyC(lamc,lamcm,fic,ficm,vec);
fin1=fic*diag(kapa1);

%implement other methods
[gr1,fir1,alphar1] =
realmassmod(fir,firm,j,lamr,lamrm,mm,hz,M1,locm,loc,1); %Parloo
[gr2,fir2,alphar2] =
realmassmod(fir,firm,j,lamr,lamrm,mm,hz,M1,locm,loc,2); %Brincker
[gr3,fir3,alphar3] =
realmassmod(fir,firm,j,lamr,lamrm,mm,hz,M1,locm,loc,3); %Bernal
Projection

%convert complex modes to real for graphical comparison
finlr=real(fin1*diag(sqrt(2*imag(lamc)*i)));
fitr=-fit*diag(sqrt(2*imag(lamct)*i));
fitr(:,1)=-fitr(:,1);

%compute ideal scaling factors
for mm=1:3
    alc(mm)=pinv(fic(:,mm))*fit(:,mm);
    alr(mm)=pinv(fir(:,mm))*fitr(:,mm);
end

alc([2 3])=-alc([2 3]);

%compute scaling error term
scaler1=(alr-alphar1)./alr;
scaler2=(alr-alphar2)./alr;
scaler3=(alr-alphar3)./alr;
scaler4=(alc-kapa1.')./alc;
scaler=real([scaler1;scaler2;scaler3;scaler4]);

```

NORMANDYC.M – (IMPLEMENTS RECEPTANCE METHOD)

```
function [kapa]=normandyC(L0,L1,fi0,fi1,mper)
nm=length(L0);
% change names to use old code
bb=L0; %complex eigenvalues (initial)
bbp=L1; %complex eigenvalues (perturbed)
aa1=fi0; %complex mode shapes (initial)
aa2=fi1; %complex mode shapes (perturbed)

% get the coefficients using the formula in the paper
for jp=1:nm;
y=[];
    for j=1:nm;
        q=aa1(:,j) .*diag(mper)*aa2(:,jp)*bbp(jp)^2/(bbp(jp)-bb(j));
yy=aa1(:,j)*q;
y=[y yy];
end;
y1{jp}=y;
end;
Y=[];
for j=1:nm;
    Y=[Y;y1{j}];
end;

% right hand side
q=length(mper);
L=aa2(:,1:nm);
L=reshape(L,q*nm,1);
kapa2=-pinv(Y)*L;
kapa=sqrt(kapa2);
```

REALMASSMOD.M – (IMPLEMENTS PARLOO, BRINCKER, AND BERNAL PROJECTION METHODS AND CALCULATES RECEPTANCE)

```

function [g,fin,alpha] =
realmassmod(fi,fim,j,lamb,lama,mm,freq,M1,locm,loc,flag1)
% loc = row and column in the FRF matrix desired
% fi=arbitrarily scaled mode shapes extracted in the ID
% lamb = vector with the eigenvalues prior to the mass modification
% lama = vector with the eigenvalues after the mass modification
% mm = mass modification
% freq = frequency axis.
% M1=vector with the diagonal of the M1 matrix
% locm= # of the sensor where the mass addition is placed.
%flag1=1 for Parloo, 2 for Brincker, 3 for Bernal projection
[tt,rr]=size(fi);
if flag1==1
for jj=1:rr;
    num=-(lama(jj)-lamb(jj))/mm;
    den1=fi(locm,jj) .*diag(M1)*fi(locm,jj);
    den2=lamb(jj);
    alp2(jj)=num/(den1*den2);
end
elseif flag1==2
for jj=1:rr;
    num=-(lama(jj)-lamb(jj))/mm;
    den1=fi(locm,jj) .*diag(M1)*fi(locm,jj);
    den2=lama(jj);
    alp2(jj)=num/(den1*den2);
end
else
    k=diag(pinv(fi)*fim);
for jj=1:rr;
    num=-(lama(jj)-lamb(jj))/mm*k(jj);
    den1=fi(locm,jj) .*diag(M1)*fim(locm,jj);
    den2=lama(jj);
    alp2(jj)=num/(den1*den2);
end;
end
alpha=sqrt(alp2);
fin=fi*diag(alpha);
w=freq*2*pi;
s=w*1i;

%calculate transfer function for desired input and output
for dd=1:length(s);
    G=zeros(tt);
for jj=1:rr
qq=s(dd)^2*fin(:,jj)*fin(:,jj) ./ (s(dd)^2+2*sqrt(lamb(jj))*j(jj)*s(dd)+
lamb(jj));
    G=G+qq;
end;
    g(dd)=G(loc(1),loc(2));
end;

```